OXFORD

Cerebral Cortex, 2022, **00**, 1–17
https://doi.org/10.1093/cercor/bhab514
Original Article

Developmental Maturation of Causal Signaling Hubs in Voluntary Control of Saccades and Their Functional Controllability

Yuan Zhang[1,†], Srikanth Ryali[1,†], Weidong Cai[1], Kaustubh Supekar[1], Ramkrishna Pasumarthy[2], Aarthi Padmanabhan[1], Bea Luna[3,4] and Vinod Menon[1,5,6]

[1]Department of Psychiatry and Behavioral Sciences, Stanford University School of Medicine, Stanford, CA 94305, USA
[2]Department of Electrical Engineering, Robert Bosch Center of Data Sciences and Artificial Intelligence, Network Systems Learning, Control and Evolution Group, Indian Institute of Technology Madras, Chennai 600036, India
[3]Department of Psychiatry and Behavioral Sciences, University of Pittsburgh, Pittsburgh, PA 15213, USA
[4]Department of Psychology, University of Pittsburgh, Pittsburgh, PA 15213, USA
[5]Department of Neurology & Neurological Sciences, Stanford University School of Medicine, Stanford, CA 94305, USA
[6]Wu Tsai Neuroscience Institute, Stanford University School of Medicine, Stanford, CA 94305, USA
Address correspondence to Vinod Menon, PhD. Email: menon@stanford.edu

[†]Yuan Zhang and Srikanth Ryali contributed equally to this work

Abstract

The ability to adaptively respond to behaviorally relevant cues in the environment, including voluntary control of automatic but inappropriate responses and deployment of a goal-relevant alternative response, undergoes significant maturation from childhood to adulthood. Importantly, the maturation of voluntary control processes influences the developmental trajectories of several key cognitive domains, including executive function and emotion regulation. Understanding the maturation of voluntary control is therefore of fundamental importance, but little is known about the underlying causal functional circuit mechanisms. Here, we use state-space and control-theoretic modeling to investigate the maturation of causal signaling mechanisms underlying voluntary control over saccades. We demonstrate that directed causal interactions in a canonical saccade network undergo significant maturation between childhood and adulthood. Crucially, we show that the frontal eye field (FEF) is an immature causal signaling hub in children during control over saccades. Using control-theoretic analysis, we then demonstrate that the saccade network is less controllable in children and that greater energy is required to drive FEF dynamics in children compared to adults. Our findings provide novel evidence that strengthening of causal signaling hubs and controllability of FEF are key mechanisms underlying age-related improvements in the ability to plan and execute voluntary control over saccades.

Keywords: causal circuits, controllability, frontal eye fields, inhibitory control, saccades

Introduction

Voluntary control over saccades plays an important role in directing visuospatial attention, detecting and tracking salient objects in space, forming priority maps of visual images, and in selective visual attention to stimuli that are relevant to behavior (Moore and Fallah 2001; Moore and Zirnsak 2017). The ability to adaptively respond to behaviorally relevant cues in the environment undergoes significant maturation from childhood to adulthood (Schachar and Logan 1990; Williams et al. 1999). Adaptive and flexible behaviors involve suppression of automatic but inappropriate responses and deployment of an alternative response, based on goal-relevant contextual cues (Munoz and Everling 2004). These voluntary control processes are thought to be immature in children (Diamond 2013). A prime example of this in a laboratory setting is the antisaccade (AS) task, which has been widely used to probe brain systems underlying voluntary control over eye movements (Curtis et al. 2005; Ford et al. 2005; Brown et al. 2006; Ettinger et al. 2008; Cai, Cannistraci, et al. 2014a). In the AS task, participants are required to make a saccadic eye movement away from a target presented in the peripheral visual field, suppressing the natural tendency to make reflexive saccades toward it (Munoz and Everling 2004). Children find this task particularly difficult, not because they fail to understand the task rules but because of difficulty in suppressing automatic responses to the target, which is consistent with evidence for immature inhibitory control processes in childhood (Fischer et al. 1997; Fukushima et al. 2000; Klein and Foerster 2001). More generally, several lines of evidence suggest that planning eye movements and directing visuospatial attention share overlapping brain mechanisms and investigations of saccades have a long history in nonhuman primate studies arising from their central role in selective visual attention (Moore and Fallah 2001;

Received: August 17, 2021. **Revised:** December 14, 2021. **Accepted:** December 15, 2021

Moore and Zirnsak 2017). Thus, investigations of brain circuits involved in voluntary control of saccades also have the potential to inform mechanisms underlying immature context-sensitive orienting to salient visual stimuli in the environment.

Neuroimaging studies of saccadic control in humans have shown consistent recruitment of a canonical saccade network involving prefrontal control regions including FEF, anterior insula, anterior cingulate cortex, inferior frontal gyrus and presupplementary motor area as well as subcortical regions including the basal ganglia and cerebellum (Munoz and Wurtz 1993; Gaymard et al. 1998; Schall 2002; Curtis et al. 2005; Ford et al. 2005; McHaffie et al. 2005; Brown et al. 2006; Dyckman et al. 2007; Leung and Cai 2007; Ettinger et al. 2008; Hwang et al. 2010; Domagalik et al. 2012; Krauzlis et al. 2013; Cai, Cannistraci, et al. 2014a; Chen et al. 2016; Basso and May 2017; Jarvstad and Gilchrist 2019). In contrast to distributed brain areas identified in human functional magnetic resonance imaging (fMRI) studies, electrophysiological studies in nonhuman primates have targeted the FEF as a key cortical region involved in the control and execution of saccades (Schall and Hanes 1993; Schall et al. 1995; Hanes et al. 1998; Everling and Munoz 2000; Curtis et al. 2005; Izawa et al. 2005; Ohayon et al. 2013). Electrophysiological studies in monkeys have discovered movement and fixation neurons in the FEF that are specifically associated with eye movement execution and inhibition (Hanes et al. 1998; Schall 2002). The specific role of the FEF and dynamic circuit mechanisms that guide integration of information between the FEF and other distributed brain areas implicated in voluntary control over saccades and, crucially, their developmental maturation is largely unknown (Supekar and Menon 2012; Chen et al. 2015; Cai et al. 2016, 2017). In particular, little is known about the maturation of causal circuits associated with the FEF and other prefrontal cortex regions implicated in inhibitory control. Here we seek to advance knowledge of the developmental maturation of dynamic causal brain circuits involved in voluntary control over saccades with several novel computational tools, including state-space modeling, network science, and control theory, which has allowed us to address critical gaps in the literature.

Our study addresses three major gaps in the literature on the developmental maturation of dynamic functional circuits involved in voluntary control over saccades. Our first goal was to investigate the developmental maturation of dynamic causal interactions in brain circuits associated with voluntary control over saccades (Fig. 1; Hwang et al. 2010). We operationalized dynamic causal interactions as follows: A brain region has a causal influence on a target if the past history of temporal signals predicts the target's signal, consistent with the formulation used in most dynamic causal modeling studies (Friston et al. 2003; Roebroeck et al. 2005; Seth 2005; Ryali et al. 2011). Specifically, we used a novel multivariate dynamic state-space identification (MDSI) model (Ryali et al. 2011; Ryali, Chen et al. 2016a; Ryali, Shih, et al. 2016b) to characterize directed causal interactions between nodes of a canonical saccade control network during an AS task and that during a control prosaccade (PS) task involving involuntary saccades to visual targets. A previous study using Granger causal analysis revealed that mature inhibitory control is supported by top-down cortical–subcortical influences during saccade processing (Hwang et al. 2010). However, Granger causal analysis cannot accurately estimate causal interactions as it does not take into account regional variation in the hemodynamic response function, which can significantly impact inferences made about the direction of causal signaling (Ryali et al. 2011). For example, a brain region that is active early but has a slower hemodynamic response might be observed in fMRI signals to be active later than an area with an opposite profile (Ryali et al. 2011; Ryali, Chen et al. 2016a; Ryali, Shih, et al. 2016b). Furthermore, Granger causal analysis cannot accurately resolve causal influences specific to each task condition as it requires concatenating noncontinuous time series data. Therefore, the context-specific causal circuit mechanisms and signaling hubs underlying control over saccades remain poorly understood. Our study overcomes these methodological challenges using state-space models that allow the estimation of unobserved dynamics: in our case, latent signals that give rise to the observed fMRI signals which evolve over time (Ryali et al. 2011; Dubin and Koopman 2012; Ryali, Chen et al. 2016a; Ryali, Shih, et al. 2016b). Discrete-time state-space models are widely used to investigate temporal dynamics in biological time series and were first introduced to fMRI time series analysis by our group. Our approach is conceptually similar to dynamic causal models (Friston et al. 2003) with two essential differences: First, MDSI is based on well-developed methods for discrete time series and second, it jointly estimates the strength of causal links without having to test a large number of models. We hypothesized that, compared with adults, children would show immature patterns of causal interactions during the AS, but not the PS, task.

The second goal of our study was to identify causal signaling hubs in the saccade control network and determine whether these hubs are immature in children. Hubs are highly connected regions important for the integration of activity across brain regions (Tomasi and Volkow 2011; van den Heuvel and Sporns 2013). The weighted directed graphs estimated by MDSI allowed us to compute hubs from both the perspective of outflow from, and inflow into, each node of the network as a function of the task context. Based on extant neurophysiological studies (Hanes et al. 1998; Moore and Armstrong 2003), we hypothesized that the FEF would emerge as a causal control hub in both children and adults and that children would show significantly weaker outflow from the FEF when compared with adults. We contrast this profile with other prefrontal cortex regions that regulate hierarchical cognitive control (Badre and Nee 2018).

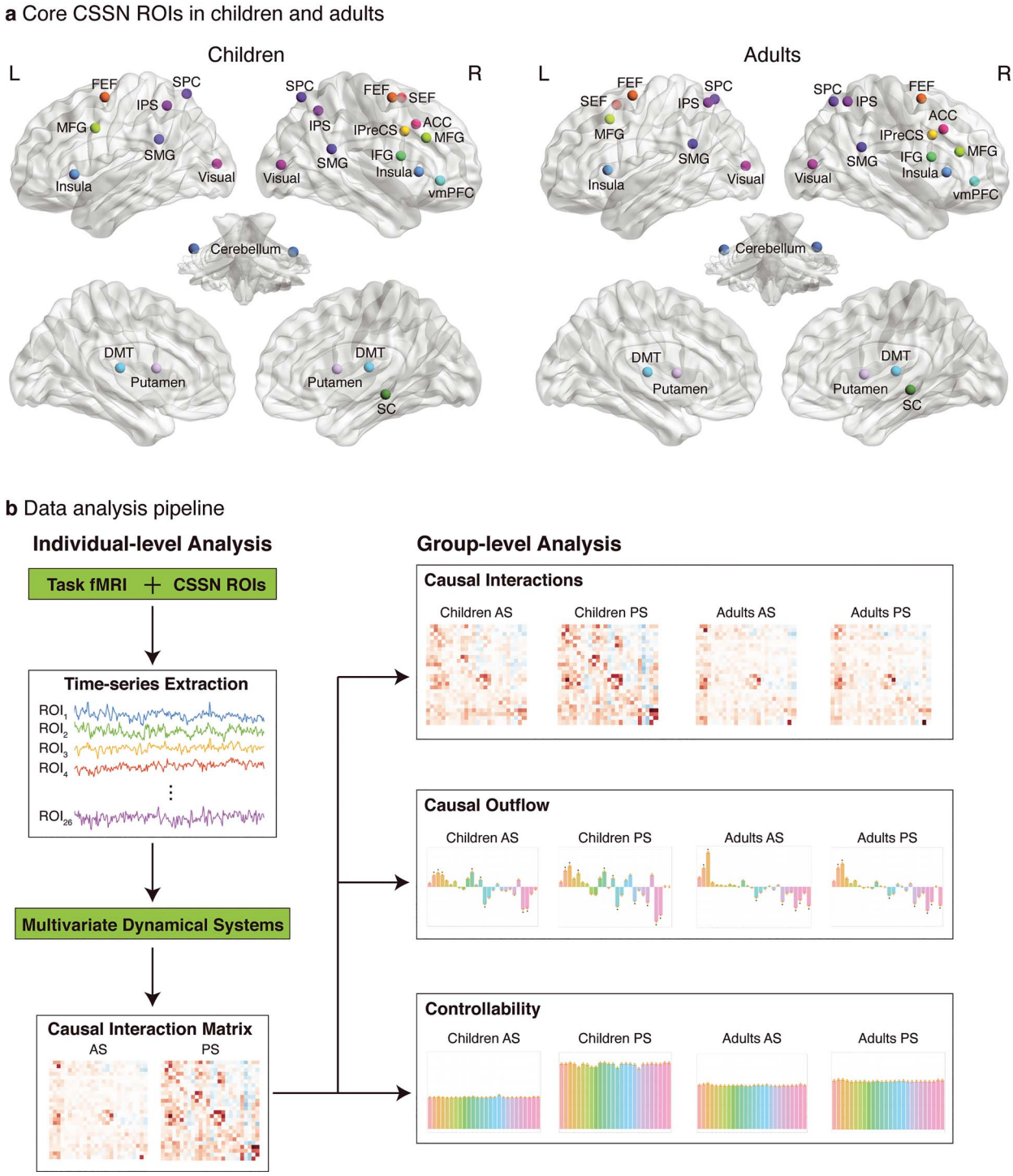

Figure 1. Saccade control network and data analysis pipeline. (*a*) Twenty-six brain regions comprising the cortical–subcortical saccade control network (Table 2). (*b*) Overview of the data analysis pipeline. Task fMRI time series were extracted and analyzed using a state-space multivariate dynamical systems identification (MDSI) model to estimate task-specific causal interactions between network nodes during the AS and PS tasks. The resulting directed (asymmetric) causal interactions were used to determine causal outflow and functional network controllability in each node. At the group level, multivariate classification and ANOVA were used to assess developmental changes in causal interactions, causal outflow, and controllability during the AS and PS tasks.

The third goal of our study was to assess functional controllability of the saccade network and determine whether key nodes of the saccade network are less controllable in children as compared with adults. Our MDSI model naturally lends itself to innovative analysis of functional controllability, a powerful technique that combines models of circuit dynamics to provide a metric of the extent of influence of a set of brain nodes over other brain nodes across changing states associated with the PS and AS tasks. Functional controllability is a key index of control in complex systems, which has been applied to many disciplines of physics, engineering, and

biology (Liu et al. 2011; Liu and Barabasi 2016; Yan et al. 2017). Control properties of complex systems can provide novel insights into how they can be perturbed to achieve desired behaviors (Lombardi and Hornquist 2007; Ruths and Ruths 2014; Tang and Bassett 2018). Controllability, in the classical sense, measures the ability to perturb a system from a given initial state to random target states, in finite time, by means of external control inputs. Crucially, nodes with higher controllability require lower energy for perturbing a system from its current state (Leitold et al. 2017) and controllability measures are useful for identifying driver nodes, which have the potential to influence overall system dynamics (Liu et al. 2011). Previous applications of control theory to human neuroimaging were based on structural brain connectivity derived using diffusion tensor imaging and are ill suited for assessing cognitive context–dependent effects in functional networks (Sojoudi and Doyle 2014; Gu et al. 2015; Tu et al. 2018). We recently developed a metric for functional controllability and identified frontal cognitive control circuits that operate asymmetrically during working memory in adults (Cai et al. 2021). Here, we apply these recently developed functional network controllability measures to identify, for the first time, nodes that need the lowest energy to perturb the saccadic control network, and to compare functional network controllability in children and adults. We hypothesized that functional networks would be more difficult to control in children compared to adults, with more energy needed for voluntary control over saccades in children. Based on microstimulation studies in nonhuman primates emphasizing a causal role for the FEF in saccadic control (Schlag-Rey et al. 1992; Munoz and Wurtz 1993; Burman and Bruce 1997; Moore and Armstrong 2003; Moore and Fallah 2004), we further hypothesized that functional controllability of the FEF is weaker in children, which reflects immature voluntary control over saccades.

To our knowledge, these methodological innovations have never been applied to the study of functional circuits involved in the voluntary control of saccades and their developmental maturation. Critically, our study advances knowledge of the developmental maturation of dynamic causal brain circuits involved in voluntary control over saccades with several novel computational tools and bridges critical gaps between human and nonhuman primate literature on functional circuitry and developmental maturation of the FEF.

Materials and Methods

Saccade Task Dataset

Overview

The dataset used in this study was identical to the one used in a previous study (Hwang et al. 2010). fMRI data were preprocessed using FSL, including realignment, slice-timing correction, coregistration to subjects' structural T1 images and normalization to a 2 mm MNI152 template, smoothing with a 5 mm full-width half-maximum Susan kernel, high-pass filtering, and grand mean intensity normalization. Details of the data acquisition protocols, fMRI preprocessing, and activation analyses are described therein. Briefly, data from 71 healthy controls, comprising 35 children (8–13 years; 21 female) and 36 adults (19–29 years; 18 female), were included in the study (see demographic information in Table 1). All participants were native English speakers with no history of neurological or psychiatric conditions in themselves or a first-degree relative as established by interview. All participants had normal or corrected-to-normal vision. All participants had normal full-scale intelligence quotients, and these did not differ between age groups (mean IQ: children, 107.3; adults, 111.5; $p > 0.05$). During fMRI scanning they performed an event-related experiment with two task conditions. In the PS task, they were instructed to look toward a target stimulus presented on the screen; in the AS task they were instructed to look opposite to the location of target. A general linear model was used to identify AS task-related activation peaks. Activated peaks within 10 mm radius of peaks from a theoretically defined template were selected as regions of interest (ROIs). The final set of ROIs consisted of 26 core cortical–subcortical saccadic network nodes (Fig. 1*a*). Mean fMRI time series of the 26 saccade network nodes were extracted from each participant, detrended, *Z*-normalized, and used for MDSI analysis to examine causal interactions among the saccade network nodes for correctly performed trials on the AS and PS task conditions. Corrective saccades were not examined due to insufficient corrective saccade trials in most participants.

Table 1. Participant characteristics for children and adults

	Children ($n = 35$)	Adults ($n = 36$)
Age (years)		
Mean ± std	11.1 ± 1.4	20.8 ± 2.3
Range	8.1–13.0	19.1–28.9
Female/male	21/14	18/18
IQ	107.3 ± 9.1	111.5 ± 9.6

fMRI Task Design

Within AS and PS task blocks, the duration of intervals between task trials was jittered. For AS trials, participants were instructed to look toward a point on the screen opposite the location of a peripheral target stimulus. For PS trials, participants were instructed to look toward the target stimulus. Each task block (AS and PS) consisted of 12 trials, with a total of 48 AS and 48 PS trials across runs. Each trial began with a 3 s fixation cross-hair (subtending ~0.7° of visual angle). The cross-hair color could be green, cueing participants to make a prosaccade or red for cueing an antisaccade. Each target stimulus was a solid yellow circle, subtending approximately 0.5°, and was presented on the horizontal meridian at one of

Table 2. MNI coordinates of the 26 saccadic control network ROIs for children and adults

Region	MNI coordinates (children)			MNI coordinates (adults)		
	x	y	z	x	y	z
SEF	1.84	7.48	59.64	−2.53	10.35	56.06
R FEF	28.88	0.13	59.9	29.97	1.3	60.89
L FEF	−28.38	−3.36	60.1	−28.34	−1.99	63.33
R IPreCS	50.14	9.62	33.95	55.53	9.54	32.74
L MFG	−53.56	3.94	36.28	−39.43	15.56	44.97
R MFG	52.19	26.34	28.9	43.42	30.79	19.64
R IFG	59.63	6.83	15.01	61.8	9.07	15.88
vmPFC	12.84	37.01	−3.98	3.11	42.4	−3.23
R insula	38.91	20.61	2.8	40	20.71	3.89
L insula	−36.76	20.03	0.78	−35.61	17.26	5.52
ACC	6.96	18.5	39.41	9.09	18.3	37.15
R SMG	59.83	−46.35	20.27	64.19	−44.96	23.42
L SMG	−56.78	−45.18	27.75	−60.04	−48.59	25.9
R SPC	21.5	−69.65	60.21	22.56	−66.56	58.76
L SPC	−16.29	−66.38	62.77	−17.41	−65.53	60.46
R IPS	34.3	−56.61	49.74	30.09	−55.79	58.69
L IPS	−31.58	−51.21	53.69	−26.1	−60.45	57.87
R putamen	22.84	6.28	11.21	22.79	5.87	6.77
L putamen	−21.46	8.25	11.77	−20.42	3.59	7.73
R DMT	13.2	−18.32	12.69	12.08	−18.63	9.38
L DMT	−12.74	−19.58	12.14	−10.62	−18.82	8.66
SC	5.4	−31.06	−8.33	6.52	−29.68	−5.12
R Cere	37.71	−61.22	−22.7	35.55	−65.58	−23.36
L Cere	−35.78	−69.34	−25.13	−32.5	−63.59	−21.27
R Visual	13.31	−85.3	8.11	13.33	−82.96	10.12
L Visual	−5.04	−89.62	8.85	−2.87	−89.61	8.81

six unpredictable eccentricities (at ±3, 6 or 9°). Fixation periods between trials varied from 3 to 9 s (2–6 volumes). Each task block ended with a 3 s "task end" cue indicating that a long period of fixation would follow.

ROIs

Left hemisphere and right hemisphere regions of interest for both groups are shown in Figure 1*a*, and coordinates of each ROI are listed in Table 2. Twenty-six regions known to be involved in oculomotor control and response inhibition were selected based on anti-saccade task-related activation and their well-known role in cognitive control, as described by Hwang and colleagues (Hwang et al. 2010). Cortical nodes consisted of the oculomotor regions, including the supplementary eye field (SEF), bilateral FEF, right inferior precentral sulcus (IPreCS), bilateral IPS, bilateral superior parietal cortex (SPC), and bilateral supramarginal gyrus (SMG); prefrontal cortical regions implicated in cognitive control, working memory, and response inhibition, including the bilateral middle frontal gyrus (MFG), right inferior frontal gyrus (IFG), bilateral insula, and anterior cingulate cortex (ACC). Subcortical nodes consisted of bilateral basal ganglia (putamen), bilateral dorsal medial thalamus (DMT), the superior colliculus (SC), and the cerebellum (Cere).

MDSI Model for Estimating Causal Interactions from fMRI Data

MDSI estimates context-dependent causal interactions between multiple brain regions in latent quasi-neuronal states while accounting for variations in hemodynamic responses in these regions. MDSI has been validated using extensive simulations (Ryali et al. 2011; Ryali, Chen et al. 2016a; Ryali, Shih, et al. 2016b) and has been successfully applied to our previous studies (Supekar and Menon 2012; Chen et al. 2015; Cai et al. 2016, 2021). MDSI models the multivariate fMRI time series by the following state-space equations:

$$\boldsymbol{s}(t) = \sum_{j=1}^{J} v_j(t) C_j \boldsymbol{s}\,(t-1) + \boldsymbol{w}(t) \tag{1}$$

$$\boldsymbol{x}_m(t) = [\boldsymbol{s}_m(t)\ \boldsymbol{s}_m\,(t-1) \ldots . \boldsymbol{s}_m\,(t-L+1)]' \tag{2}$$

$$y_m(t) = b_m \Phi \boldsymbol{x}_m(t) + \boldsymbol{e}_m(t) \tag{3}$$

In equation (1), $\boldsymbol{s}(t)$ is a $M \times 1$ vector of latent quasi-neuronal signals at time t of M regions, A is an $M \times M$ connection matrix wherein C_j is an $M \times M$ connection matrix ensued by modulatory input $v_j(t)$and J is the number of modulatory inputs. The nondiagonal elements of C_j represent the coupling of brain regions in the presence of modulatory input $v_j(t)$. $C_j(m, n)$ denotes the strength of causal connection from the nth region to the mth region for the jth type stimulus. Therefore, latent signals $\boldsymbol{s}(t)$ in M regions at time t is a bilinear function of modulatory inputs $v_j(t)$, corresponding to deviant or standard stimulus and its previous state, $\boldsymbol{s}(t-1)$. $\boldsymbol{w}(t)$ is an $M \times 1$ state noise vector whose distribution is assumed to be

Gaussian distributed with covariance matrix $Q(\boldsymbol{w}(t) \sim N(0, Q))$. Additionally, state noise vector at time instances $1,2,\ldots,T$ $(\boldsymbol{w}(1), \boldsymbol{w}(2) \ldots \boldsymbol{w}(T))$ are assumed to be identical and independently distributed (iid). Equation (1) represents the time evolution of latent signals in M brain regions. More specifically, the latent signals at time t, $\boldsymbol{s}(t)$, is expressed as a linear combination of latent signals at time $t-1$, external stimulus at time t $(u(t))$, bilinear combination of modulatory inputs $v_j(t), j = 1, 2..J$ and its previous state, and state noise $\boldsymbol{w}(t)$. The latent dynamics modeled in equation (1) gives rise to observed fMRI time series represented by equations (2) and (3).

We model the fMRI time series in region *"m"* as a linear convolution of hemodynamic response function (HRF) and latent signal $\boldsymbol{s}_m(t)$ in that region. To represent this linear convolution model as an inner product of two vectors, the past L values of $\boldsymbol{s}_m(t)$ are stored as a vector. $\boldsymbol{x}_m(t)$ in equation (2) represents an $L \times 1$ vector with L past values of latent signal at the mth region.

In equation (3), $y_m(t)$ is the observed blood oxygen level-dependent (BOLD) signal at t of the mth region. Φ is a $p \times L$matrix whose rows contain bases for HRF. b_m is a $1 \times p$ coefficient vector representing the weights for each basis function in explaining the observed BOLD signal $y_m(t)$. Therefore, the HRF in mth region is represented by the product $b_m\Phi$.The BOLD response in this region is obtained by convolving HRF $(b_m\Phi)$ with the L past values of the region's latent signal $(\boldsymbol{x}_m(t))$ and is represented mathematically by the vector inner product $b_m\Phi\ \boldsymbol{x}_m(t)$. Uncorrelated observation noise $\boldsymbol{e}_m(t)$ with zero mean and variance $\sigma_m^2$is then added to generate the observed signal $y_m(t)$. $\boldsymbol{e}_m(t)$ is also assumed to be uncorrelated with $\boldsymbol{w}(\tau)$,at all t and τ. Equation (3) represents the linear convolution between the embedded latent signal $\boldsymbol{x}_m(t)$ and the basis vectors for HRF. Here, we use the canonical HRF and its time derivative as bases as is common in most fMRI studies.

Equations (1)–(3) together represent a state-space model for estimating the causal interactions in latent signals based on the observed multivariate fMRI time series. Furthermore, the MDSI model also takes into account variations in HRF as well as the influences of modulatory and external stimuli in estimating causal interactions between the brain regions.

Estimating causal interactions between M regions specified in the model is equivalent to estimating the parameters $C_j, j = 1, 2..J$. In order to estimate C_js, the other unknown parameters Q, $\{b_m\}_{m=1}^{M}$ and $\{\sigma_m^2\}_{m=1}^{M}$ and the latent signal $\{\boldsymbol{s}(t)\}_{t=1}^{T}$ based on the observations $\left\{y_m^s(t)\right\}_{m=1,s=1}^{M,S}, t = 1, 2..T$, where T is the total number of time samples and S is number of subjects, need to be estimated. We use a variational Bayes approach (VB) for estimating the posterior probabilities of the unknown parameters of the MDSI model given fMRI time series observations for S number of subjects.

State-Space Analysis of Dynamic Causal Interactions

Extensive computer simulations on previously published benchmark datasets, as well as more realistic neurophysiological models, have demonstrated that MDSI can accurately estimate dynamic causal interactions in fMRI data (Ryali et al. 2011; Ryali, Chen et al. 2016a; Ryali, Shih, et al. 2016b). To prepare data for MDSI analysis, the fMRI time series from each ROI and participant were first linearly detrended and then normalized by its standard deviation. For all ROIs, time series were extracted using the MarsBar toolbox in SPM8. Spherical ROIs were defined as the sets of voxels contained in 6 mm (diameter) spheres centered on the MNI coordinates of each ROI. MDSI was applied to estimate directed causal interactions among 26 nodes separately in the AS and PS tasks.

Graph-Theoretical Analysis

To characterize the causal network interactions generated by MDSI, we evaluated net causal influences of each saccade network node and determined causal outflow from each node during the AS and PS tasks in each participant. Specifically, we computed the outflow degree of each node in each task and participant by subtracting averaged inflow weights (all the input connections to a node from all other nodes) from averaged outflow weights (all the output connections from a node to all other nodes).

Network Controllability

Dynamic control processes related to functional brain network organization are modeled as a linear, discrete, time invariant systems of the form

$$x\left(k+1\right) = A\ x(k) + Bu(k),$$

where x denotes the state vector, A is the weighted task-specific connectivity matrix estimated by MDSI, with elements of the matrix A describing connectivity between various nodes of the network, and u denotes the control inputs. The input matrix B identifies control nodes or regions in the brain. Controllability here refers to the ability of the system to transfer from a given initial state to any target state, in finite time, by means of an external control input. In the context of brain networks, it means the ability to drive the brain to specific states that facilitate adaptive behaviors and cognition.

Classical results from control theory suggest that a system is controllable if and only if there exists a unique positive definite solution W to the Lyapunov equation:

$$AW + WA' + BB' = 0$$

.

In particular the unique positive solution takes the form

$$W = \sum_{\tau=0}^{\infty} A^{\tau} BB' (A')^{\tau}$$

This positive definite matrix W is often referred to as the controllability Grammian. In addition to verifying whether the system is controllable or not, the Grammian can be used to assign a value to each node, or a set of nodes (or community modules), which quantifies the influence of each node/module over the entire network.

Multivariate Classification Analysis of Dynamic Causal Interactions Between Groups and Between Tasks

To determine whether causal networks associated with the AS and PS tasks differ between children and adults during each task, we used the causal network patterns in the two groups. The dynamic causal interaction patterns—MDSI weights of 325 pairs of anatomical regions—were used as the input (features) to a linear logistic regression classifier. The classifier distinguishes the children AS from adult AS tasks by fitting a separating hyperplane between the classes. K-fold cross-validation ($K = 10$) was used to measure the performance of the classifier in distinguishing children AS and adult AS tasks. In K-fold, 1-fold is used for testing the classifier that is trained using the remaining $K - 1$ folds. This process is repeated K times. The entire K-fold cross-validation procedure was repeated 20 times. These analyses were performed using the scikit-learn package (https://scikit-learn.org/), which is a Python-based package for machine learning. Permutation tests (200 permutations of class labels) were conducted to arrive at P values associated with classification accuracy. Similar procedures were used to determine whether networks associated with the PS task differ between children and adults.

To examine whether causal networks associated with the AS and PS tasks differ in each group, we applied the aforementioned analysis to the MDSI-estimated causal networks during AS and PS tasks for each group.

Multivariate Classification Analysis of Regional Causal Outflow Between Groups and Between Tasks

Similarly, we applied the aforementioned analysis to causal outflow patterns to examine whether causal outflow associated with the AS and PS tasks differ between children and adults during each task and differ between the AS and PS tasks in each group.

Multivariate Classification Analysis of Network Controllability Between Groups and Between Tasks

Finally, we applied the aforementioned analysis to network controllability patterns to examine whether controllability associated with the AS and PS tasks differ between children and adults during each task and differ between the AS and PS tasks in each group.

Statistical Analysis

To examine how task performance was modulated by group and task, we performed a two-way mixed measures analysis of variance (ANOVA) on accuracy and latency separately, with the between-subject factor group (children vs adults) and the within-subject factor task (AS vs PS). Upon significant group by task interaction, post-hoc paired t-tests and two-sample t-tests were performed.

To identify causal outflow and inflow hubs, we performed a one-sample t-test on causal outflow for each node and results were FDR corrected. In order to examine how outflow and inflow hubs were modulated by group and task, for each hub region we performed a two-way mixed measures ANOVA with the between-subject factor group and within-subject factor task. Upon significant group by task interaction, post-hoc paired t-tests and two-sample t-tests were performed.

To examine how network controllability was modulated by group and task across nodes, we performed a three-way ANOVA with the between-subject factor group and within-subject factors task and node for controllability. Upon significant group by task interaction, post-hoc paired t-tests and two-sample t-tests were performed for each node and results were FDR corrected. Two-way ANOVAs on controllability with the between-subject factor group and within-subject factor task were also performed for outflow hub regions, and post-hoc paired t-tests and two-sample t-tests were performed upon significant group by task interaction.

Results

Behavioral Performance in Children Compared to Adults

A two-way mixed measures analysis of variance (ANOVA) on performance accuracy with the between-subject factor group (children vs. adults) and within-subject factor task (AS vs. PS) revealed a significant interaction between group and task ($F_{1,69} = 45.44$, $P < 0.001$, Eta-squared = 0.24) and main effects of group ($F_{1,69} = 53.15$, $P < 0.001$, Eta-squared = 0.28) and task ($F_{1,69} = 319.92$, $P < 0.001$, Eta-squared = 0.70). Post-hoc paired t-tests revealed that performance accuracy was significantly lower for the AS task compared to the PS task in both children (AS: $45 \pm 17\%$; PS: $96 \pm 5\%$; $t_{34} = -16.31$, $P < 0.001$, Cohen's $d = 2.76$) and adults (AS: $74 \pm 17\%$; PS: $97 \pm 3\%$; $t_{35} = -8.58$, $P < 0.001$, Cohen's $d = 1.43$; Supplementary Fig. 1). Post-hoc two-sample t-tests revealed that, in comparison to adults, children had significantly lower accuracy for the AS ($t_{69} = -7.22$, $P < 0.001$, Cohen's $d = 1.71$) but not the PS task ($t_{69} = -1.45$, $P = 0.15$; Supplementary Fig. 1).

A two-way mixed measures ANOVA on mean saccade latencies with the factors group and task revealed no significant interaction between group and task

($F_{1,69} = 0.05$, $P = 0.82$) but significant main effects of group ($F_{1,69} = 6.07$, $P = 0.016$, Eta-squared = 0.06) and task ($F_{1,69} = 291.44$, $P < 0.001$, Eta-squared = 0.55). Post-hoc paired *t*-tests revealed that latency was significantly longer for the AS task compared to the PS task in both children (AS: 517 ± 91 ms; PS: 389 ± 41 ms; $t_{34} = 10.21$, $P < 0.001$, Cohen's $d = 1.73$) and adults (AS: 486 ± 55 ms; PS: 361 ± 29 ms; $t_{35} = 15.55$, $P < 0.001$, Cohen's $d = 2.59$; Supplementary Fig. 1). Post-hoc two-sample *t*-tests revealed that, in comparison to adults, children had significantly longer latency for the PS ($t_{69} = 3.24$, $P = 0.002$, Cohen's $d = 0.77$) but not the AS task ($t_{69} = 1.73$, $P = 0.09$; Supplementary Fig. 1).

These results suggest that both children and adults show better task performance (higher accuracy and shorter latency) during the PS, compared to the AS, task and that children show lower levels of accuracy than adults in the AS but not the PS task.

Differentiation of Dynamic Causal Circuit Patterns Between Children and Adults

We assessed dynamic causal interactions in a saccade control network known to be consistently implicated in a variety of oculomotor control tasks (Curtis et al. 2005; Ford et al. 2005; Ettinger et al. 2008; Cai, Cannistraci, et al. 2014a). Twenty-six regions known to be involved in oculomotor control, response inhibition, and cognitive control were chosen based on procedures described previously (Hwang et al. 2010; Fig. 1*a*). We first investigated whether multivariate patterns of causal interactions differed between children and adults in the AS and PS tasks (Fig. 2). A logistic regression classifier revealed significant developmental differences between causal interaction patterns engaged in both the AS (accuracy = 74.9%; $P < 0.005$, permutation test; Fig. 2*a*) and PS (accuracy = 80.3%; $P < 0.005$, permutation test; Fig. 2*b*) tasks (Supplementary Table 1).

These results suggest that children engage different patterns of causal circuits during performance of the AS and PS tasks, when compared to adults.

Saccade-Related Causal Outflow and Inflow Hubs in Children and Adults

We then sought to identify causal signaling hubs during the AS and PS tasks in children and, separately, in adults. We evaluated net causal influences of each saccade network node and determined the net causal outflow from each node during the AS and PS tasks in each participant. Specifically, we computed the outflow degree of each node in each task and participant by subtracting averaged inflow weights (all the input connections to a node from all other nodes) from averaged outflow weights (all the output connections from a node to all other nodes).

In children, we found that prefrontal cortex regions including bilateral FEF, right inferior precentral sulcus, and anterior cingulate cortex (ACC), as well as parietal regions including left supramarginal gyrus, showed significant positive outflow ($P < 0.05$, FDR corrected; Fig. 3*a*) during the AS task, with the ACC and FEF showing the highest outflow degree ($P < 0.001$, FDR corrected). Similarly, prefrontal cortex regions including bilateral FEF, left middle frontal gyrus, and anterior cingulate cortex, as well as parietal regions including left supramarginal gyrus, showed significant positive outflow ($P < 0.05$, FDR corrected; Fig. 3*b*) during the PS task, with the left FEF showing the highest outflow degree ($P < 0.001$, FDR corrected). In adults, we found that frontal regions including the left and right FEF showed significant positive outflow ($P < 0.05$, FDR corrected) during both the AS (Fig. 3*a*) and PS (Fig. 3*b*) tasks, with the left FEF showing the highest outflow degree (AS: $P < 0.0001$, FDR corrected; PS: $P < 0.002$, FDR corrected).

In children, we found that the bilateral cerebellum and right superior parietal cortex showed significant inflow ($P < 0.05$, FDR corrected) during both the AS (Fig. 3*a*) and PS (Fig. 3*b*) tasks, with the cerebellum showing the highest inflow degree ($P < 0.0001$, FDR corrected). In adults, we found that the bilateral cerebellum, left visual area, right dorsomedial thalamus, and right SPC showed significant inflow ($P < 0.05$, FDR corrected) during both the AS (Fig. 3*a*) and PS (Fig. 3*b*) tasks with the right cerebellum showing the highest inflow degree ($P < 0.0001$, FDR corrected).

These results suggest that FEF is a causal outflow hub and cerebellum is a causal inflow hub in the saccade control network during the AS and PS tasks in both children and adults.

Differentiation of Causal Outflow and Inflow Patterns Between Children and Adults

Next, we examined whether multivariate patterns of causal outflow and inflow differed between children and adults in the AS and PS tasks. We found that children and adults showed significant differences between regional causal outflow and inflow patterns engaged during the AS (accuracy = 62.3%; $P = 0.025$, permutation test; Fig. 3*a*) and PS (accuracy = 62.5%; $P = 0.002$, permutation test; Fig. 3*b*) tasks (Supplementary Table 1).

Additionally, we examined whether multivariate patterns of causal outflow and inflow differed between the AS and PS tasks in each group. We found that children showed significant differences between causal outflow and inflow patterns engaged during the AS and PS tasks (accuracy = 62.9%; $P = 0.01$, permutation test), which stands in contrast to adults who showed no differentiation between the AS and PS causal outflow and inflow patterns (accuracy = 57.0%; $P = 0.13$, permutation test) (Supplementary Table 1).

These results suggest that the regional causal outflow and inflow patterns associated with the AS and PS tasks undergo significant developmental changes from childhood to adulthood and that, unlike adults, children engage different patterns of regional causal outflow and inflow between the two tasks.

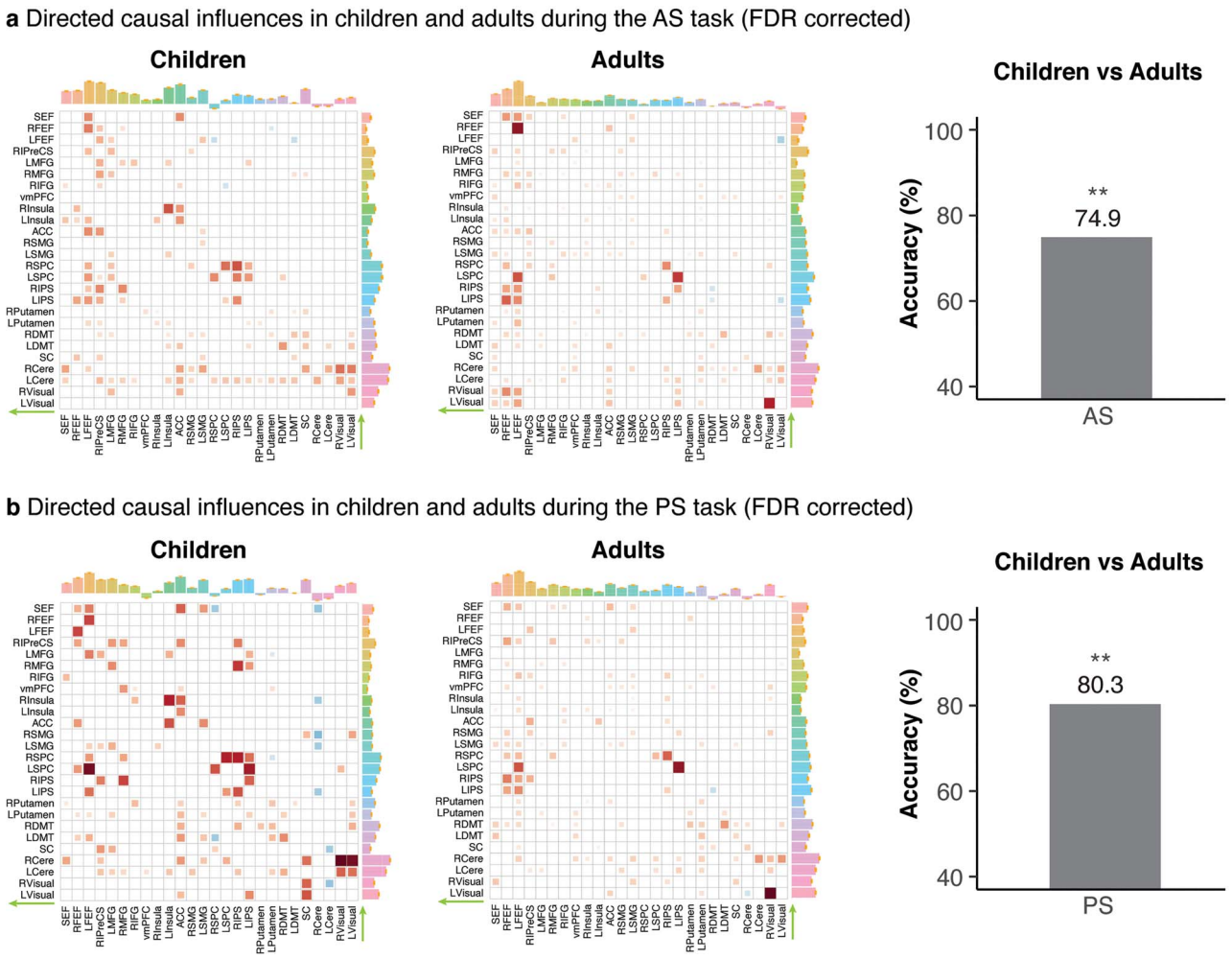

Figure 2. Causal network interactions during both AS and PS tasks are immature in children. Significant directed causal influences between saccade network nodes in children and adults during (*a*) the AS task and (*b*) the PS task ($P < 0.05$, FDR corrected). Accuracy of multivariate classification between groups for each task are shown in bar plots. Red cells in the matrices indicate significant positive influences, and blue indicates significant negative influences. Bar plots on the top of each matrix indicate the strength of causal outflow in each ROI and that on the right of each matrix indicate the strength of causal inflow in each ROI. $^{**}P < 0.01$.

Task-Dependent FEF Network Outflow in Children Compared to Adults

Because the FEF emerged as a causal outflow hub in the saccade network, we then specifically examined whether its task-dependent network outflow differed between children and adults. We conducted an ANOVA with between-subject factor group (children vs. adults) and within-subject factor task (AS vs. PS) for outflow of the left and right FEF separately.

In the left FEF, we found a significant group × task interaction ($F_{1,69} = 6.45$, $P = 0.013$, Eta-squared = 0.016). Paired *t*-tests revealed a higher outflow in the left FEF during the AS than the PS tasks ($t_{35} = 2.24$, $P = 0.03$, Cohen's $d = 0.37$) in adults. No such effect was found in children ($t_{34} = -1.40$, $P = 0.17$). Two-sample *t*-tests revealed that outflow in the left FEF was weaker in children than adults during the AS ($t_{69} = -2.04$, $P = 0.04$, Cohen's $d = 0.49$) but not the PS task ($t_{69} = 0.19$, $P = 0.85$; Fig. 4*a*; Supplementary Table 2). A similar analysis in the right FEF found no group effect ($F_{1,69} = 1.20$, $P = 0.28$), task effect ($F_{1,69} = 1.84$, $P = 0.18$), or their interaction ($F_{1,69} = 0.02$, $P = 0.90$) for outflow.

These results suggest that children show lower outflow than adults in the left FEF and that the outflow is less differentiated in children between the AS and PS tasks.

Task-Dependent Cerebellum Network Inflow in Children Compared with Adults

Because the cerebellum emerged as a causal inflow hub in the saccade network, we then specifically examined whether its task-dependent network inflow differed between children and adults. We conducted an ANOVA with between-subject factor group (children vs. adults) and within-subject factor task (AS vs. PS) for inflow of the left and right cerebellum separately.

We found a significant main effect of group ($F_{1,68} = 6.61$, $P = 0.012$, Eta-squared = 0.071), with higher inflow in children than adults in the left cerebellum (Fig. 4*b*;

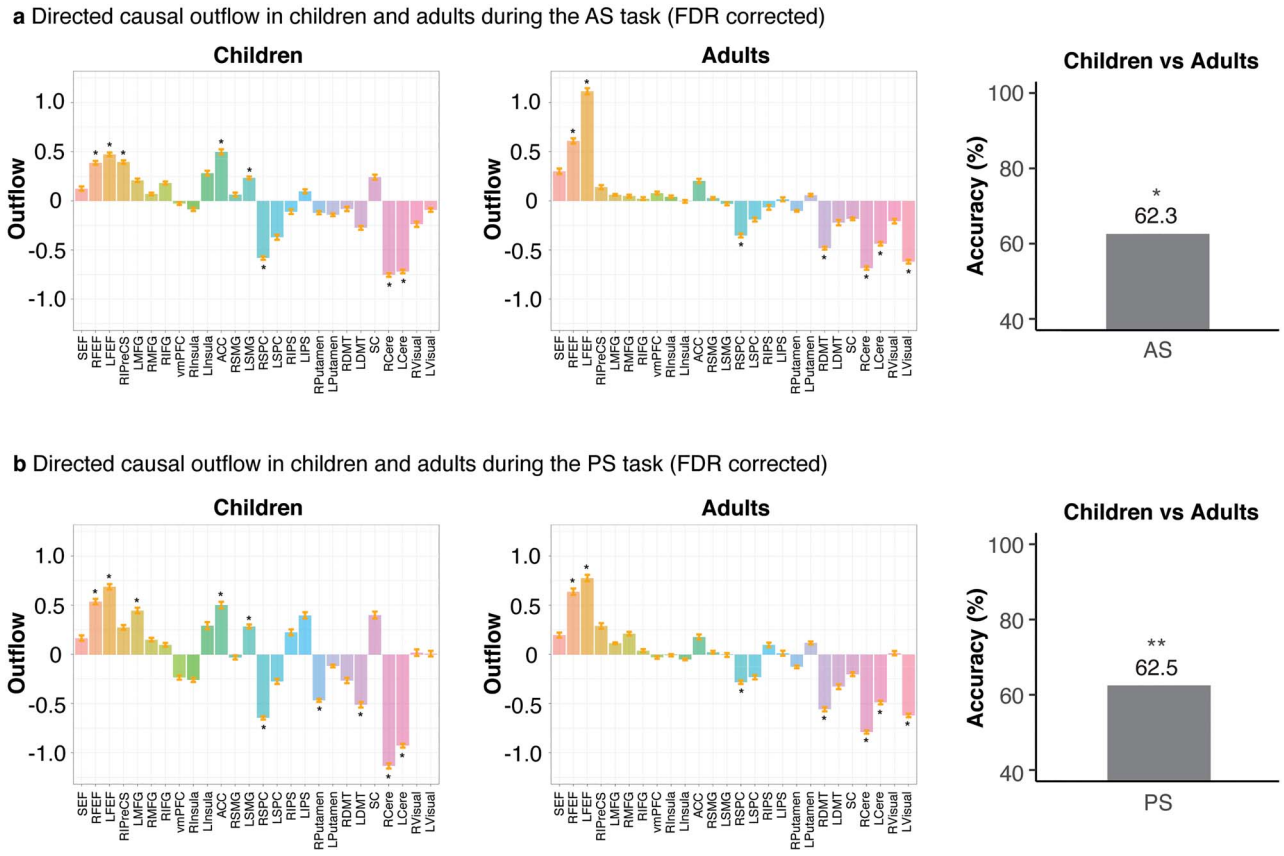

Figure 3. Causal outflow hub in FEF and immature causal signaling in children. FEF are a causal signaling hub in both children and adults during the (*a*) AS and (*b*) PS tasks. In contrast, the cerebellum emerged as a causal inflow (i.e., negative outflow) hub during both the AS and PS tasks in children and adults. Other brain areas that showed statistically significant outflow and inflow are also shown (*P <0.05, FDR corrected). Causal signaling patterns differed significantly between children and adults in both the AS and PS tasks as revealed by multivariate classification analysis. Error bar indicates standard error of the mean. * and **P <0.05 and P <0.01, respectively.

Supplementary Table 2). No main effect of Task ($F_{1,68}$ = 3.15, P = 0.08) or group × task interaction ($F_{1,68}$ = 1.15, P = 0.29) were found. A similar analysis in the right cerebellum did not reveal a main effect of group ($F_{1,67}$ = 1.80, P = 0.18) or group × task interaction ($F_{1,67}$ = 3.10, P = 0.08).

These results suggest that children show higher inflow than adults in the left cerebellum during both the AS and PS tasks.

Differentiation of Network Controllability Patterns Between Children and Adults

Next, we examined whether multivariate patterns of functional network controllability associated with the AS and PS tasks differed between children and adults in the AS and PS tasks. We found that children and adults showed significant differences between multivariate patterns of controllability engaged during the AS (accuracy = 62.2%, P = 0.01, permutation test) and PS tasks (accuracy = 58.8%; P = 0.025, permutation test) (Supplementary Fig. 2; Supplementary Table 1).

Additionally, we examined whether multivariate patterns of network controllability differed between the AS and PS tasks in each group. We found that children showed significant differences between controllability patterns engaged during the AS and PS tasks (accuracy = 77.1%; P <0.002, permutation test). In contrast, adults showed no differentiation between the AS and PS controllability patterns (accuracy = 48.6%; P = 0.67, permutation test) (Supplementary Table 1).

To further clarify group differences in functional network controllability, we conducted a three-way ANOVA with the within-subject factors task and node and the between-subject factor group for controllability. While the three-way interaction between group, task, and node was not significant ($F_{25,1725}$ = 0.84, P = 0.54), we identified a significant group × task interaction ($F_{1,69}$ = 7.25, P = 0.009, *Eta-squared* = 0.03) across nodes. Further two-sample t-tests revealed a significantly lower network controllability in children than adults in the AS task (p <0.05, FDR corrected) in all nodes (Supplementary Fig. 2*a*). No group differences were found in individual nodes during the PS task (Supplementary Fig. 2*b*). Additionally, paired t-tests revealed a significantly lower network controllability during the AS than the PS tasks in children (P <0.05, FDR corrected) whereas no task differences were found in adults (Supplementary Figs 2 and 3).

These results suggest that functional network controllability is weaker in children compared with adults and is particularly impaired in the AS task.

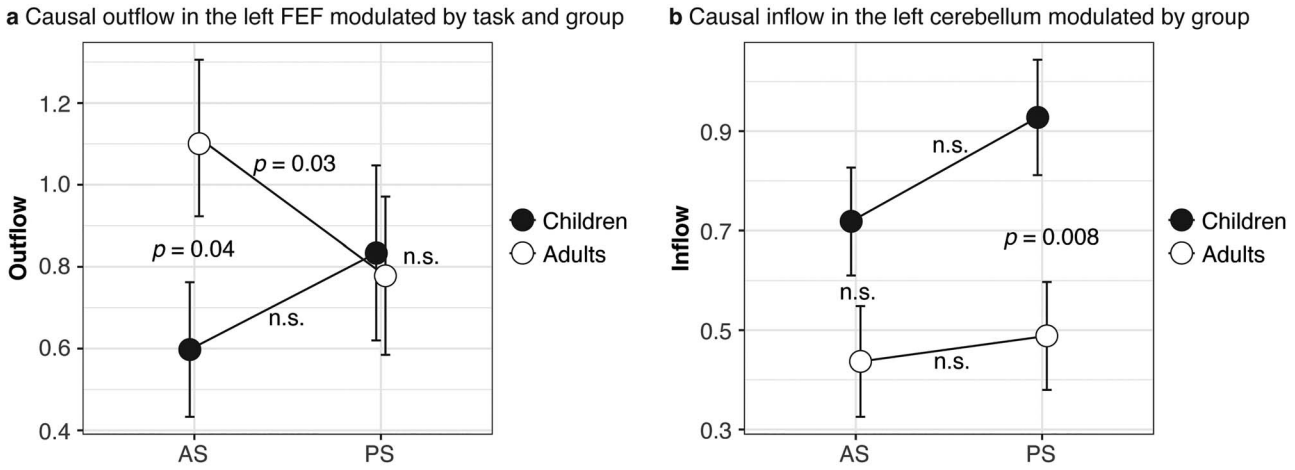

Figure 4. Immature outflow and inflow hubs in children. (*a*) Weak FEF causal outflow hub in children. Children show lower causal outflow from the FEF during the AS task compared with adults. They also show less differentiated outflow between the AS and PS tasks compared with adults. (*b*) Enhanced causal inflow hub in the cerebellum in children. Children show higher inflow during both AS and PS tasks when compared with adults. Error bar indicates standard error of the mean.

Task-Dependent FEF Network Controllability in Children Compared with Adults

Given that the FEF emerged as a causal outflow hub in the saccade network, we further examined whether its task-dependent network controllability differed between children and adults. We conducted an ANOVA with the between-subject factor group (children vs adults) and the within-subject factor task (AS vs. PS) of the left and right FEF separately.

In the left FEF, we found a significant group × task interaction ($F_{1,65} = 19.74$, $P < 0.001$, Eta-squared = 0.051). Paired *t*-tests revealed a weaker controllability in the left FEF during the AS than the PS tasks ($t_{31} = -6.88$, $P < 0.001$, Cohen's $d = 1.22$) in children. No such effect was found in adults ($t_{31} = -1.73$, $P = 0.09$). Two-sample *t*-tests revealed that controllability in the left FEF was weaker in children than adults during the AS ($t_{65} = -2.17$, $P = 0.03$, Cohen's $d = 0.53$) but not the PS task ($t_{65} = 1.68$, $P = 0.10$) (Fig. 5; Supplementary Table 3).

In the right FEF, we found a significant group × task interaction ($F_{1,65} = 18.09$, $P < 0.001$, Eta-squared = 0.045). Paired *t*-tests revealed a weaker controllability in the right FEF during the AS than the PS tasks ($t_{31} = -7.00$, $P < 0.001$, Cohen's $d = 1.24$) in children. No such effect was found in adults ($t_{31} = -1.82$, $P = 0.08$). Two-sample *t*-tests revealed that controllability in the right FEF were weaker in children than adults during the AS ($t_{65} = -2.08$, $P = 0.04$, Cohen's $d = 0.51$) but not the PS task ($t_{65} = 1.56$, $P = 0.12$) (Fig. 5; Supplementary Table 3).

These results confirm that network controllability from the FEF associated with the AS task is immature in children.

Discussion

We used several novel computational tools to uncover causal signaling mechanisms underlying the developmental maturation of brain circuits involved in voluntary control over saccadic eye movements. Our analysis focused on a canonical distributed cortical–subcortical network of brain areas important for inhibitory control of eye movements. This network included prefrontal and parietal cortical regions implicated in cognitive control, and subcortical basal ganglia, thalamus, SC, and cerebellar regions involved in gating and oculomotor control (Pierrot-Deseilligny et al. 2004; Schall and Boucher 2007). We used multivariate dynamical state-space identification (MDSI) to evaluate the maturation of network properties including causal signaling hubs. Network analysis revealed significant age-related changes between childhood and adulthood in directed causal influences and causal outflow hubs in the saccade control network. The FEF emerged as a causal outflow hub in both children and adults during both the AS and PS tasks, and outflow from the FEF was significantly weaker in children, compared with adults, during voluntary control over saccades. Our analysis further revealed inflow hubs in bilateral cerebellum in both the AS and PS tasks. Surprisingly, inflow into the lateral superior cerebellum was significantly higher in children compared with adults. Control-theoretic analyses revealed that saccade network is less controllable in children from the FEF suggesting that greater energy is required to drive frontal eye field dynamics in children compared to adults. Our findings provide novel evidence that immature causal signaling hubs and controllability of the FEF contributes to developmental maturation of voluntary control over saccades.

Causal Network Interactions During Both AS and PS tasks Are Immature in Children

The first goal of our study was to determine whether children engage an adult-like causal signaling mechanism during voluntary control of eye movements. MDSI models allowed us to investigate latent context-specific dynamic causal mechanisms underlying control of saccades in children and adults for the first time. MDSI

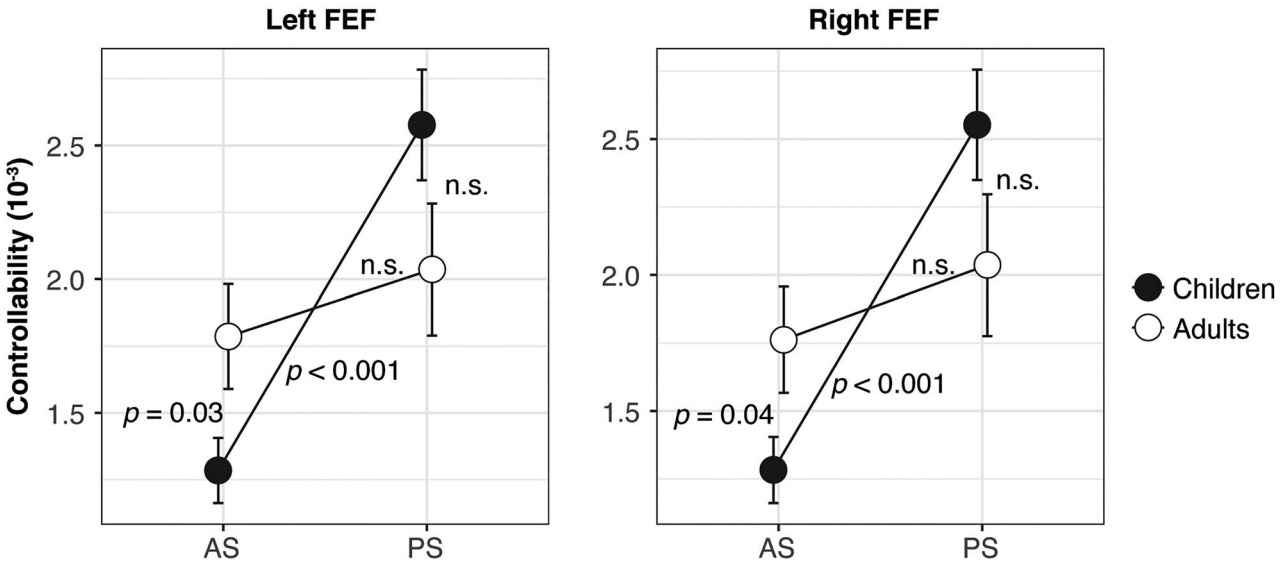

Figure 5. Weak controllability of FEF in children. Children show weak controllability in both the left and right FEF during the AS task. They also show weaker controllability in the AS compared with the PS task in contrast to adults who showed no differences between the AS and PS tasks. Error bar indicates standard error of the mean.

jointly estimated causal circuit interactions between all nodes of the saccade control networks and has several advantages for estimating context-specific causal interactions in latent neuronal space (Ryali et al. 2011; Ryali, Chen et al. 2016a; Ryali, Shih, et al. 2016b). Crucially, MDSI is a latent state space dynamic systems model that estimates task-specific causal interactions without the confounding influences of variation in hemodynamic response function across brain regions. Furthermore, MDSI does not require testing a large number of prespecified models, which is especially problematic as the number of the models to be tested increases exponentially with the number of nodes (26 in the present study). Our analysis revealed that children and adults differ significantly in the pattern of causal signaling elicited by the AS task. Surprisingly, causal interaction patterns also distinguished children from adults in the PS task, demonstrating that the cortical–subcortical saccade control network is immature during both voluntary and involuntary control of saccades in childhood. Weaker causal interaction in the AS, relative to PS (Fig. 2), task condition reflects immature modulation of the saccade network in response to the high demands of voluntary control over saccades in children. We will next unpack key mechanisms of causal signaling underlying age-related maturation of this network.

Immature Differentiation of Directed Causal Outflow Between AS and PS Tasks in Children

Next, extending network-level analysis we examined node-level measures of net directed causal outflow patterns associated with each brain region in the cortical–subcortical saccade control network. We used MDSI-derived measures of the full directed (asymmetric) connectivity matrix to determine the net causal outflow of each node measured as the difference between outflow versus inflow weights (Sridharan et al. 2008; Supekar and Menon 2012; Chen et al. 2015; Cai et al. 2016, 2021). A node with a high net causal outflow indicates that a brain region exerts greater causal influence on other nodes than other nodes exert on it whereas a high negative value indicates the reverse. Multivariate classification analysis revealed that causal outflow differed significantly in both the AS and PS tasks between children and adults. Crucially, causal outflow patterns differed significantly between the AS and PS tasks in children but not in adults. Results demonstrate that net causal outflow patterns are immature in children during both voluntary and involuntary control of saccades. Furthermore, results also reveal immature differentiation of directed causal outflow between voluntary and involuntary saccades in children. Together, these findings identify immature causal control over saccades in children.

Weak Outflow from the FEF During AS Task in Children

Our second major goal was to identify causal signaling hubs associated with the saccade control network and probe their maturation. Extending our analysis of immature differentiation in children, we first determined brain areas which play a dominant causal role in signaling within the saccade network. Our analysis revealed that, in both children and adults, the FEF is a common causal outflow hub during performance of the AS and PS tasks and provides novel evidence for a key role for this region in the developmental maturation of voluntary control over saccades.

Crucially, analysis of developmental, age-related changes revealed that the FEF was modulated by cognitive demands associated with voluntary control over saccades. Causal signaling from the FEF was

significantly weaker in children during the AS but not the PS task. Whereas adults showed higher causal outflow from the FEF during the AS than the PS task, no such task-related modulation was observed in children. Although our findings suggest that the FEF is already established as a causal hub by age 12, the strength of causal signaling from this region continues to mature into adulthood. Together, these results highlight the crucial role of FEF in inhibitory control over saccades and its immature network function in children.

Although the FEF is a key cortical region involved in control and execution of saccades (Schall and Hanes 1993; Schall et al. 1995; Hanes et al. 1998; Everling and Munoz 2000; Curtis et al. 2005; Izawa et al. 2005; Ohayon et al. 2013), its role in voluntary control of saccades has received less attention in human neuroimaging studies when compared to electrophysiological studies in non-human primates and its functional role and maturation is poorly understood in the context of human cognitive development. Electrophysiological studies in monkeys have suggested that the FEF is involved in two processes that are needed for the AS task: suppression of the automatic involuntary eye movements and inversion of the response into the correct saccade vector (Everling and Munoz 2000; Munoz and Everling 2004). In monkeys performing the AS task, saccade-responsive neurons in the FEF are inhibited before the target appears in order to suppress the automatic saccades and prevent activity in these neurons from crossing a threshold that would allow a saccade in the direction of the stimulus to be initiated (Munoz and Everling 2004). Furthermore, electrophysiological studies in monkeys have revealed that the FEF also plays a key role in vector inversion of saccade direction (Sato and Schall 2003; Basu et al. 2021). We suggest that both these saccade control processes may be immature in children.

In humans, it is surmised that multiple other prefrontal cortex regions, notably the right IFG, which implements response inhibition (Aron et al. 2014; Cai, Ryali, et al. 2014b; Cai et al. 2017) and lateral PFC regions that encode task rules (Badre and Nee 2018), are alternate candidate causal signaling hubs. However, this was not the case as the FEF emerged as a dominant causal signaling hub in both adults and children. It is interesting to consider this finding in relation to other response inhibition paradigms, such as stop-signal and go/no-go tasks. Unlike stop-signal or no-go stimuli, antisaccade trials are cued before the onset of target visual stimuli. In the current study, the AS and PS tasks were blocked and an instruction (either "Start LOOK-AWAY game" for AS blocks, or "Start LOOK-TOWARD game" for PS blocks) was presented in the beginning of each block (Hwang et al. 2010). Participants therefore needed to initiate saccadic suppression before the appearance of the target to which a vector inversion of saccades needed to be executed and a more mature system would be better capable of implementing a proactive control strategy to suppress reflexive saccades. In contrast, inhibition in the stop-signal or the go/no-go tasks is triggered by the onset of uncued stop and no-go signals and therefore likely relies on more "bottom-up" reactive control processes generally associated with the fronto-insular cortex (Cai, Ryali, et al. 2014b; Cai et al. 2017, 2019). These distinctive characteristics of the AS task may help explain the key role of the FEF detected in the present study. Thus, our results suggest that the FEF is a causal hub in the cortical–subcortical oculomotor network that proactively suppresses and then drives other oculomotor control regions to trigger anti-saccade eye movements when appropriate (Keller et al. 2008; Peel et al. 2017; Mirpour et al. 2018). The greater causal network outflow from the FEF in adults is consistent with its role in generation of vector inversion, and is likely a key neural mechanism underlying immature voluntary control over saccades in children.

Immature Inflow into the Cerebellum in Children During Antisaccades and Prosaccades

Our analysis also revealed inflow hubs in bilateral superior lateral cerebellum (Crus I) in both AS and PS tasks in children as well as adults. The cerebellum plays a crucial role in guiding smooth eye pursuit and is involved in saccade generation, adaptation, and correction (Girard and Berthoz 2005; Thier and Markanday 2019). It receives input about visual target and eye position information to make appropriate adjustments or corrections (Schweighofer et al. 1996). Indeed, lesions to the cerebellum are associated with failure in saccade adaptation and increased variability of saccade amplitude (Waespe and Baumgartner 1992; Straube et al. 2001). The higher inflow degree observed in both children and adults is consistent with its hypothesized role in fine tuning eye movements based on feedback signals from attentional, sensory, and oculomotor systems (Sokolov et al. 2017; Stephen et al. 2018; Stoodley and Schmahmann 2018; King et al. 2019).

Surprisingly, causal signaling into the cerebellum was higher in children compared with adults. Furthermore, unlike the FEF, there was no main effect of task (AS vs. PS) or group × task interaction in the cerebellum indicating that the effects are not specific to voluntary control over saccades but were common to both voluntary and involuntary saccades. Thus, our results point to greater inflow to the cerebellum required for both maintaining and altering saccades in children. The cerebellum receives signals from multiple cortical and subcortical regions and acts as a "comparator" between planned and actual movement (Stein and Glickstein 1992; Flament and Ebner 1996). The higher inflow degree observed in children suggests that stronger signals from attentional, sensory, and oculomotor systems may be required to maintain amplitude of saccades, hold gaze patterns and avoid choppy pursuits, which are typically considered hallmarks of cerebellar oculomotor function (Leigh and Zee 2015; Salman and Tsai 2016). Further studies are

needed to investigate the precise mechanisms underlying greater top-town cortical–subcortical influence on the cerebellum in children and how this leads to maturation of oculomotor function and control over saccades from childhood to adulthood.

Weak Controllability of Causal Saccade Networks in Children

The third goal of our study was to determine whether the saccadic network is equally controllable by external inputs in children, when compared to adults. Specifically, we used average controllability, measured as the trace of controllability Grammian W_t, as our quantitative metric for controllability (Pasqualetti et al. 2014). In the context of functional brain networks, average controllability quantifies the influence of each node or module over the entire network, with higher controllability reflecting lower average control energy needed to drive networks from a given node or a set of nodes. Our novel approach here examines cognitive context-dependent controllability and emphasizes the importance of causal system dynamics in saccadic control (Sojoudi and Doyle 2014; Gates and Rocha 2016). We found a significant task effect on maturation of network controllability. Specifically, the saccade network was less controllable in children during the AS, compared with the PS task, which was in contrast to adults who show equal levels of network controllability in the AS and PS tasks ($P < 0.05$, FDR corrected). Children also showed significantly lower network controllability in all saccade network nodes in the AS task compared with adults. These results suggest that higher input energy (Cai et al. 2021) is required to modulate the saccade network during voluntary control of saccades, relative to execution of involuntary saccades in children but not adults.

Notably, given the crucial role of the FEF as a key cortical node in saccade control in humans and nonhuman primates (Schall and Hanes 1993; Schall et al. 1995; Hanes et al. 1998; Everling and Munoz 2000; Curtis et al. 2005; Izawa et al. 2005; Ohayon et al. 2013), and its identification as a causal outflow hub in the present study, we specifically examined whether functional controllability of the FEF was immature in children. Our analysis revealed a significant group by task interaction with lower controllability in the AS, but not the PS, task. Notably, children showed dramatically lower controllability of the FEF during the AS task. This result demonstrates that greater energy is required to drive children's saccade network from the FEF during voluntary control over saccades.

Our findings have implications for how manipulations of the FEF may impact distributed brain circuits involved in the control of saccades. Research in nonhuman primates has emphasized a causal role for the FEF in saccadic control and visual perception and attention systems (Moore and Zirnsak 2017). Microstimulation of the FEF activates SC neurons (Schlag-Rey et al. 1992) resulting in initiation or suppression of saccadic eye movements (Schlag-Rey et al. 1992; Munoz and Wurtz 1993; Burman and Bruce 1997). FEF microsimulation has also been shown to result in direct changes in primary visual cortex neural activity (Moore and Armstrong 2003; Moore and Fallah 2004). Reversible inactivation of the FEF reduces neuronal activity in the SC (Veniero et al. 2021) and interferes with generation of saccades (Sommer and Tehovnik 1997; Dias and Segraves 1999). In humans, single-pulse transcranial magnetic stimulation over the FEF increases neural excitability in multiple visual cortical areas and modulates visual perception (Veniero et al. 2021). Our findings of lower controllability of the FEF in children suggests that stimulation of this region may have less influence on multiple distributed cortical and subcortical regions involved in saccadic control and spatial attention. Together, results demonstrate that network controllability is immature in children and further highlight novel mechanisms of immature network function associated with voluntary control over eye movements. Further studies with causal circuit manipulation techniques such as transcranial magnetic stimulation are needed to determine whether changes to FEF excitability alters top-down control over saccades similarly in children and adults.

Conclusion

State-space modeling and network analysis uncovered mechanisms underlying the operation of a core cortical–subcortical saccadic control network in children and adults and revealed multiple aspects of causal circuit dysfunction in children. We identified causal outflow and inflow hubs reflecting asymmetries in how canonical saccadic control network operates during voluntary control of saccades. Control-theoretic measures revealed a significant role for the FEF in influencing other nodes in the saccade network and driving network dynamics. Importantly, we found that the maturation of voluntary control over saccades from childhood to adulthood is associated with the strengthening of causal signaling hubs and functional controllability of the FEF. More broadly, our computational approach drawing on state-space modeling, network science, and control theory provides new tools for probing the maturation of cognitive and inhibitory control in the human brain and their dysfunction in neurodevelopmental disorders.

Supplementary Material

Supplementary material can be found at *Cerebral Cortex* online.

Funding

National Institutes of Health (HD074652 to S.R., MH105625 to W.C., EB022907 to V.M., NS086085 to V.M., MH121069 to V.M.); Indo-U.S. Science and Technology Forum (IUSSTF/JC-110/2019 to R.P.).

Notes

We thank Dr Kai Hwang for valuable feedback on an earlier draft. *Conflict of Interest*: The authors declare no competing interests.

References

Aron AR, Robbins TW, Poldrack RA. 2014. Inhibition and the right inferior frontal cortex: one decade on. *Trends Cogn Sci*. 18:177–185.

Badre D, Nee DE. 2018. Frontal cortex and the hierarchical control of behavior. *Trends Cogn Sci*. 22:170–188.

Basso MA, May PJ. 2017. Circuits for action and cognition: a view from the superior colliculus. *Annu Rev Vis Sci*. 3:197–226.

Basu D, Sendhilnathan N, Murthy A. 2021. Neural mechanisms underlying the temporal control of sequential saccade planning in the frontal eye field. *Proc Natl Acad Sci U S A*. 118:e2108922118.

Brown MRG, Goltz HC, Vilis T, Ford KA, Everling S. 2006. Inhibition and generation of saccades: rapid event-related fMRI of prosaccades, antisaccades, and nogo trials. *NeuroImage*. 33:644–659.

Burman DD, Bruce CJ. 1997. Suppression of task-related saccades by electrical stimulation in the primate's frontal eye field. *J Neurophysiol*. 77:2252–2267.

Cai W, Cannistraci CJ, Gore JC, Leung HC. 2014a. Sensorimotor-independent prefrontal activity during response inhibition. *Hum Brain Mapp*. 35:2119–2136.

Cai W, Ryali S, Chen T, Li CS, Menon V. 2014b. Dissociable roles of right inferior frontal cortex and anterior insula in inhibitory control: evidence from intrinsic and task-related functional parcellation, connectivity, and response profile analyses across multiple datasets. *J Neurosci*. 34:14652–14667.

Cai WD, Chen TW, Ryali S, Kochalka J, Li CSR, Menon V. 2016. Causal interactions within a frontal-cingulate-parietal network during cognitive control: convergent evidence from a multisite-multitask investigation. *Cereb Cortex*. 26:2140–2153.

Cai WD, Chen TW, Ide JS, Li CSR, Menon V. 2017. Dissociable fronto-operculum-insula control signals for anticipation and detection of inhibitory sensory cues. *Cereb Cortex*. 27:4073–4082.

Cai W, Duberg K, Padmanabhan A, Rehert R, Bradley T, Carrion V, Menon V. 2019. Hyperdirect insula-basal-ganglia pathway and adult-like maturity of global brain responses predict inhibitory control in children. *Nat Commun*. 10:4798.

Cai WD, Ryali S, Pasumarthy R, Talasila V, Menon V. 2021. Dynamic causal brain circuits during working memory and their functional controllability. *Nat Commun*. 12:3314.

Chen T, Michels L, Supekar K, Kochalka J, Ryali S, Menon V. 2015. Role of the anterior insular cortex in integrative causal signaling during multisensory auditory-visual attention. *Eur J Neurosci*. 41:264–274.

Chen M, Li B, Guang J, Wei LY, Wu S, Liu Y, Zhang MS. 2016. Two subdivisions of macaque LIP process visual-oculomotor information differently. *Proc Natl Acad Sc U S A*. 113:E6263–E6270.

Curtis CE, Cole MW, Rao VY, D'Esposito M. 2005. Canceling planned action: an fMRI study of countermanding saccades. *Cereb Cortex*. 15:1281–1289.

Diamond A. 2013. Executive functions. *Annu Rev Psychol*. 64:135–168.

Dias EC, Segraves MA. 1999. Muscimol-induced inactivation of monkey frontal eye field: effects on visually and memory-guided saccades. *J Neurophysiol*. 81:2191–2214.

Domagalik A, Beldzik E, Fafrowicz M, Oginska H, Marek T. 2012. Neural networks related to pro-saccades and anti-saccades revealed by independent component analysis. *NeuroImage*. 62:1325–1333.

Dubin J, Koopman S. 2012. *Time series analysis by stats space methods*. Oxford: Oxford University Press.

Dyckman KA, Camchong J, Clementz BA, McDowell JE. 2007. An effect of context on saccade-related behavior and brain activity. *NeuroImage*. 36:774–784.

Ettinger U, Ffytche DH, Kumari V, Kathmann N, Reuter B, Zelaya F, Williams SCR. 2008. Decomposing the neural correlates of anti-saccade eye movements using event-related fMRI. *Cereb Cortex*. 18:1148–1159.

Everling S, Munoz DP. 2000. Neuronal correlates for preparatory set associated with pro-saccades and anti-saccades in the primate frontal eye field. *J Neurosci*. 20:387–400.

Fischer B, Biscaldi M, Gezeck S. 1997. On the development of voluntary and reflexive components in human saccade generation. *Brain Res*. 754:285–297.

Flament D, Ebner T. 1996. The cerebellum as comparator: increases in cerebellar activity during motor learning may reflect its role as part of an error detection/correction mechanism. *Behav Brain Sci*. 19:447–448.

Ford KA, Goltz HC, Brown MR, Everling S. 2005. Neural processes associated with antisaccade task performance investigated with event-related FMRI. *J Neurophysiol*. 94:429–440.

Friston KJ, Harrison L, Penny W. 2003. Dynamic causal modelling. *NeuroImage*. 19:1273–1302.

Fukushima J, Hatta T, Fukushima K. 2000. Development of voluntary control of saccadic eye movements. I. Age-related changes in normal children. *Brain and Development*. 22:173–180.

Gates AJ, Rocha LM. 2016. Control of complex networks requires both structure and dynamics. *Sci Rep*. 6:1–16.

Gaymard B, Ploner CJ, Rivaud S, Vermersch AI, Pierrot-Deseilligny C. 1998. Cortical control of saccades. *Exp Brain Res*. 123:159–163.

Girard B, Berthoz A. 2005. From brainstem to cortex: computational models of saccade generation circuitry. *Prog Neurobiol*. 77:215–251.

Gu S, Pasqualetti F, Cieslak M, Telesford QK, Yu AB, Kahn AE, Medaglia JD, Vettel JM, Miller MB, Grafton ST, et al. 2015. Controllability of structural brain networks. *Nat Commun*. 6:8414.

Hanes DP, Patterson WF 2nd, Schall JD. 1998. Role of frontal eye fields in countermanding saccades: visual, movement, and fixation activity. *J Neurophysiol*. 79:817–834.

Hwang K, Velanova K, Luna B. 2010. Strengthening of top-down frontal cognitive control networks underlying the development of inhibitory control: a functional magnetic resonance imaging effective connectivity study. *J Neurosci*. 30:15535–15545.

Izawa Y, Suzuki H, Shinoda Y. 2005. Initiation and suppression of saccades by the frontal eye field in the monkey. *Ann N Y Acad Sci*. 1039:220–231.

Jarvstad A, Gilchrist ID. 2019. Cognitive control of saccadic selection and inhibition from within the core cortical saccadic network. *J Neurosci*. 39:2497–2508.

Keller EL, Lee BT, Lee KM. 2008. Frontal eye field signals that may trigger the brainstem saccade generator. *Prog Brain Res*. 171:107–114.

King M, Hernandez-Castillo CR, Poldrack RA, Ivry RB, Diedrichsen J. 2019. Functional boundaries in the human cerebellum revealed by a multi-domain task battery. *Nat Neurosci*. 22:1371–1378.

Klein C, Foerster F. 2001. Development of prosaccade and antisaccade task performance in participants aged 6 to 26 years. *Psychophysiology*. 38:179–189.

Krauzlis RJ, Lovejoy LP, Zenon A. 2013. Superior colliculus and visual spatial attention. *Annu Rev Neurosci*. 36:165–182.

Leigh RJ, Zee DS. 2015. *The neurology of eye movements*. New York: Oxford University Press.

Leitold D, Vathy-Fogarassy A, Abonyi J. 2017. Controllability and observability in complex networks - the effect of connection types. *Sci Rep*. 7:151.

Leung HC, Cai WD. 2007. Common and differential ventrolateral prefrontal activity during inhibition of hand and eye movements. *J Neurosci*. 27:9893–9900.

Liu YY, Barabasi AL. 2016. Control principles of complex systems. *Rev Mod Phys*. 88:035006.

Liu YY, Slotine JJ, Barabasi AL. 2011. Controllability of complex networks. *Nature*. 473:167–173.

Lombardi A, Hornquist M. 2007. Controllability analysis of networks. *Phys Rev E*. 75:056110.

McHaffie JG, Stanford TR, Stein BE, Coizet W, Redgrave P. 2005. Subcortical loops through the basal ganglia. *Trends Neurosci*. 28: 401–407.

Mirpour K, Bolandnazar Z, Bisley JW. 2018. Suppression of frontal eye field neuronal responses with maintained fixation. *Proc Natl Acad Sci U S A*. 115:804–809.

Moore T, Armstrong KM. 2003. Selective gating of visual signals by microstimulation of frontal cortex. *Nature*. 421:370–373.

Moore T, Fallah M. 2001. Control of eye movements and spatial attention. *Proc Natl Acad Sci U S A*. 98:1273–1276.

Moore T, Fallah M. 2004. Microstimulation of the frontal eye field and its effects on covert spatial attention. *J Neurophysiol*. 91: 152–162.

Moore T, Zirnsak M. 2017. Neural mechanisms of selective visual attention. *Annu Rev Psychol*. 68:47–72.

Munoz DP, Everling S. 2004. Look away: the anti-saccade task and the voluntary control of eye movement. *Nat Rev Neurosci*. 5: 218–228.

Munoz DP, Wurtz RH. 1993. Fixation cells in monkey superior colliculus. II. Reversible activation and deactivation. *J Neurophysiol*. 70:576–589.

Ohayon S, Grimaldi P, Schweers N, Tsao DY. 2013. Saccade modulation by optical and electrical stimulation in the macaque frontal eye field. *J Neurosci*. 33:16684–16697.

Pasqualetti F, Zampieri S, Bullo F. 2014. Controllability metrics, limitations and algorithms for complex networks. *IEEE Trans Control Netw Syst*. 1:40–52.

Peel TR, Dash S, Lomber SG, Corneil BD. 2017. Frontal eye field inactivation diminishes superior colliculus activity, but delayed saccadic accumulation governs reaction time increases. *J Neurosci*. 37:11715–11730.

Pierrot-Deseilligny C, Milea D, Muri RM. 2004. Eye movement control by the cerebral cortex. *Curr Opin Neurol*. 17:17–25.

Roebroeck A, Formisano E, Goebel R. 2005. Mapping directed influence over the brain using granger causality and fMRI. *NeuroImage*. 25:230–242.

Ruths J, Ruths D. 2014. Control profiles of complex networks. *Science*. 343:1373–1376.

Ryali S, Supekar K, Chen T, Menon V. 2011. Multivariate dynamical systems models for estimating causal interactions in fMRI. *NeuroImage*. 54:807–823.

Ryali S, Chen T, Supekar K, Tu T, Kochalka J, Cai W, Menon V. 2016a. Multivariate dynamical systems-based estimation of causal brain interactions in fMRI: group-level validation using benchmark data, neurophysiological models and human connectome project data. *J Neurosci Methods*. 268:142–153.

Ryali S, Shih YY, Chen T, Kochalka J, Albaugh D, Fang Z, Supekar K, Lee JH, Menon V. 2016b. Combining optogenetic stimulation and fMRI to validate a multivariate dynamical systems model for estimating causal brain interactions. *NeuroImage*. 132:398–405.

Salman MS, Tsai P. 2016. The role of the pediatric cerebellum in motor functions, cognition, and behavior: a clinical perspective. *Neuroimaging Clin N Am*. 26:317–329.

Sato TR, Schall JD. 2003. Effects of stimulus-response compatibility on neural selection in frontal eye field. *Neuron*. 38:637–648.

Schachar R, Logan GD. 1990. Impulsivity and inhibitory control in normal development and childhood psychopathology. *Dev Psychol*. 26:710–720.

Schall JD. 2002. The neural selection and control of saccades by the frontal eye field. *Philos Trans R Soc Lond Ser B Biol Sci*. 357: 1073–1082.

Schall JD, Boucher L. 2007. Executive control of gaze by the frontal lobes. *Cogn Affect Behav Neurosci*. 7:396–412.

Schall JD, Hanes DP. 1993. Neural basis of saccade target selection in frontal eye field during visual search. *Nature*. 366:467–469.

Schall JD, Hanes DP, Thompson KG, King DJ. 1995. Saccade target selection in frontal eye field of macaque. I. Visual and premovement activation. *J Neurosci*. 15:6905–6918.

Schlag-Rey M, Schlag J, Dassonville P. 1992. How the frontal eye field can impose a saccade goal on superior colliculus neurons. *J Neurophysiol*. 67:1003–1005.

Schweighofer N, Arbib MA, Dominey PF. 1996. A model of the cerebellum in adaptive control of saccadic gain. I. The model and its biological substrate. *Biol Cybern*. 75:19–28.

Seth AK. 2005. Causal connectivity of evolved neural networks during behavior. *Network*. 16:35–54.

Sojoudi S, Doyle J. 2014. Study of the brain functional network using synthetic data. *Ann Allerton Conf*. 1:350–357.

Sokolov AA, Miall RC, Ivry RB. 2017. The cerebellum: adaptive prediction for movement and cognition. *Trends Cogn Sci*. 21: 313–332.

Sommer MA, Tehovnik EJ. 1997. Reversible inactivation of macaque frontal eye field. *Exp Brain Res*. 116:229–249.

Sridharan D, Levitin DJ, Menon V. 2008. A critical role for the right fronto-insular cortex in switching between central-executive and default-mode networks. *Proc Natl Acad Sci U S A*. 105: 12569–12574.

Stein JF, Glickstein M. 1992. Role of the cerebellum in visual guidance of movement. *Physiol Rev*. 72:967–1017.

Stephen R, Elizabeth Y, Christophe H. 2018. Participation of the caudal cerebellar lobule IX to the dorsal attentional network. *Cerebellum Ataxias*. 5:9.

Stoodley CJ, Schmahmann JD. 2018. Functional topography of the human cerebellum. *Handb Clin Neurol*. 154:59–70.

Straube A, Deubel H, Ditterich J, Eggert T. 2001. Cerebellar lesions impair rapid saccade amplitude adaptation. *Neurology*. 57: 2105–2108.

Supekar K, Menon V. 2012. Developmental maturation of dynamic causal control signals in higher-order cognition: a neurocognitive network model. *PLoS Comput Biol*. 8:e1002374.

Tang E, Bassett DS. 2018. Colloquium: control of dynamics in brain networks. *Rev Mod Phys*. 90:031003.

Thier P, Markanday A. 2019. Role of the vermal cerebellum in visually guided eye movements and visual motion perception. *Annu Rev Vis Sci*. 5:247–268.

Tomasi D, Volkow ND. 2011. Functional connectivity hubs in the human brain. *NeuroImage*. 57:908–917.

Tu C, Rocha RP, Corbetta M, Zampieri S, Zorzi M, Suweis S. 2018. Warnings and caveats in brain controllability. *NeuroImage*. 176: 83–91.

van den Heuvel MP, Sporns O. 2013. Network hubs in the human brain. *Trends Cogn Sci*. 17:683–696.

Veniero D, Gross J, Morand S, Duecker F, Sack AT, Thut G. 2021. Top-down control of visual cortex by the frontal eye fields through oscillatory realignment. *Nat Commun*. 12:1757.

Waespe W, Baumgartner R. 1992. Enduring dysmetria and impaired gain adaptivity of saccadic eye movements in Wallenberg's lateral medullary syndrome. *Brain*. 115(Pt 4): 1123–1146.

Williams BR, Ponesse JS, Schachar RJ, Logan GD, Tannock R. 1999. Development of inhibitory control across the life span. *Dev Psychol*. 35:205–213.

Yan G, Vertes PE, Towlson EK, Chew YL, Walker DS, Schafer WR, Barabasi AL. 2017. Network control principles predict neuron function in the *Caenorhabditis elegans* connectome. *Nature*. 550: 519–523.